NASA
Technical
Paper
2544

December 1985

Dynamic Response of Film Thickness in Spiral-Groove Face Seals

Eliseo DiRusso

NASA

NASA Technical Paper 2544

1985

Dynamic Response of Film Thickness in Spiral-Groove Face Seals

Eliseo DiRusso

Lewis Research Center
Cleveland, Ohio

NASA

National Aeronautics and Space Administration

Scientific and Technical Information Branch

Summary

Tests were performed to experimentally determine the dynamic characteristics of the film thickness for an inward- and an outward-pumping spiral-groove face seal. The objectives were to determine the dynamic response of the film thickness for controlled motions of the seal seat and also to gain insight into the effect of secondary seal friction on film thickness behavior. A "variable-friction secondary seal" was used to remotely vary the secondary seal friction while the tests were in progress. The tests were performed with ambient air at room temperature and atmospheric pressure. The pressure drop across the seal faces was zero. The seal face load was nominally 73 N (16.4 lb) and was varied between 53 and 95.6 N (12 and 21.5 lb). The tangential velocity at the outside diameter of the seals ranged from 34 m/sec (113 ft/sec) at 7000 rpm to 98 m/sec (323 ft/sec) at 20 000 rpm.

The primary parameters measured in the tests were film thickness, seal seat axial motion, seal frictional torque, and film axial load. These data were digitized on a waveform analyzer and recorded on diskettes as functions of time. A waveform analyzer was used to plot the data.

The tests revealed that both the inward- and the outward-pumping seal had an excellent capability to follow pure sinusoidal axial oscillations of the seal seat. However, when the seal seat was skewed (plane of seal seat face not normal to shaft axis of rotation) the outward-pumping seal exhibited seriously degraded performance, and seal face contact occurred at lower film axial loads than for a true seal seat (plane of seal seat face normal to shaft axis of rotation). The skewed seal seat was not tested for the inward-pumping seal; however, the same results are anticipated.

The film thickness vibration response was relatively insensitive to secondary seal friction over a wide friction range, but the seal suddenly became unstable at the higher levels of secondary seal friction.

Introduction

A self-acting face seal employs hydrodynamic bearing technology to create a thin air film between the seal faces. This film enables the seal to operate in a noncontacting mode and thus greatly extends the life of the seal. Since this type of seal operates without face contact, it can be operated at much higher sliding speeds than contacting seals made of the same seal materials. Two popular types of film-generating mechanisms (located on one of the seal faces) are the Rayleigh step lift pad and spiral grooves. These mechanisms are discussed in detail in references 1 and 2. Both produce a thin film, generally of the order of 5 μm (0.2 mil). The film is generated as a result of the relative motion between the seal faces. This motion causes the sealed fluid to be pumped between the faces, and the resulting pressure rise separates the faces. Typical applications of the self-acting face seal are bearing compartments, balance pistons, and intershaft seals in gas turbine engines. Self-acting face seals have a leakage rate approximately one-tenth that of labyrinth seals. Hence they offer a great advantage over labyrinth seals in gas turbine engine performance.

Self-acting seals are, however, prone to instability or vibration of the seal faces (refs. 3 and 4). This causes the film thickness between the faces to vary with time. This behavior has been known for years and continues to be a problem. During previous tests at the Lewis Research Center (ref. 2) in which the objective was to study the dynamic behavior of self-acting seals, film vibrations were recorded in response to small nutational motions of the seal seat (rotating face of the face seal). It was surmised that the film vibrations observed in these tests could be altered or eliminated by changing the Coulomb damping (secondary seal friction) applied to the primary ring (nonrotating face of the face seal).

To further study the film thickness behavior, the rig was modified and tests were performed to induce programmed motion of the seal seat and also to remotely vary the damping applied to the primary ring. With this arrangement, the effects of Coulomb damping on film vibration could be studied, as well as the response of the film vibration to programmed motion of the seal seat. The need for experimental study of Coulomb damping effects on film vibration is discussed in references 5 to 7.

The overall objectives of the tests were

(1) To establish experimental baseline data for film vibrations in inward- and outward-pumping spiral-groove face seals under controlled motions of the seal seat

(2) To experimentally study the effect of Coulomb damping (secondary seal friction) on film vibrations

(3) To experimentally gain insight into key parameters affecting self-acting face seal dynamics in order to define problem areas for future work

The tests were conducted under the same conditions as the dynamic tests of reference 1. The test conditions were

Seal outside diameter, cm (in.)	9.4 (3.70)
Fluid medium	Ambient air
Fluid temperature, °C (°F)	21 (70)
Fluid pressure, kPa (psia)	101.3 (14.7)
Pressure drop across seal faces	0
Constant seal face load, N (lb)	73 (16.4)
Rotational speed range, rpm	7000 to 20 000
Tangential velocity, m/sec (ft/sec)	34 to 98 (113 to 323)

Apparatus

Seal Test Apparatus

The seal test apparatus (fig. 1) consisted of a vertically mounted shaft supported radially by two tilting-pad air journal bearings, 28 cm (11 in.) apart and suspended vertically from a servoactuated hydraulic cylinder. The ball thrust bearing (fig. 1) was required to interface between the rotating shaft and the nonrotating hydraulic cylinder shaft. A spherical joint accommodated misalignment between the shaft and the hydraulic cylinder. An air turbine (fig. 1) powered by shop air and mounted between the thrust bearing and the shaft was used to drive the shaft. The test seal assembly (figs. 2 and 3) consisted of four basic parts: (1) seal seat, (2) primary ring, (3) secondary seal, and (4) carrier. The seal seat was fastened

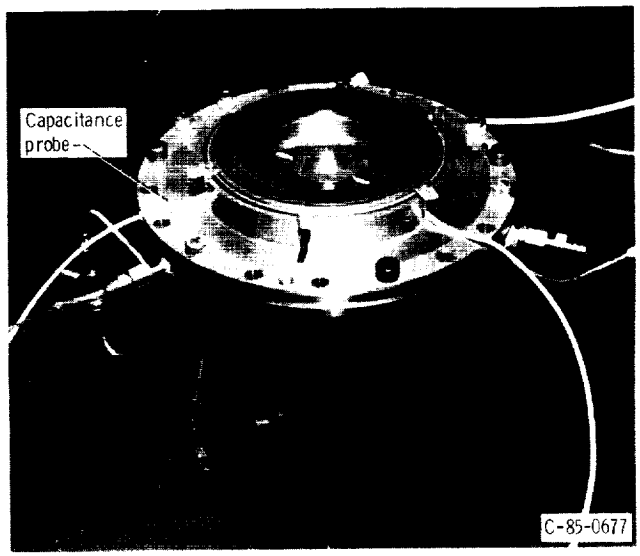

Figure 2.—Typical seal assembly.

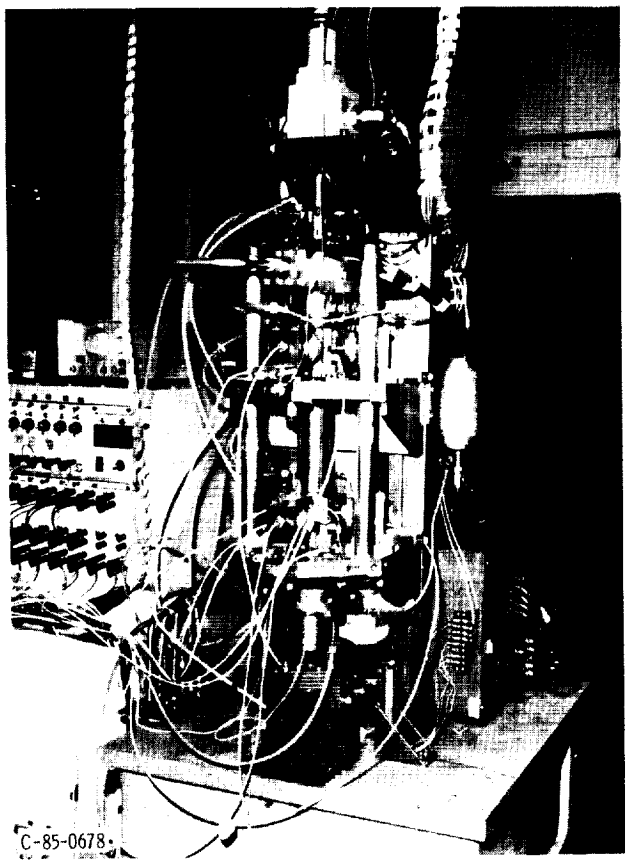

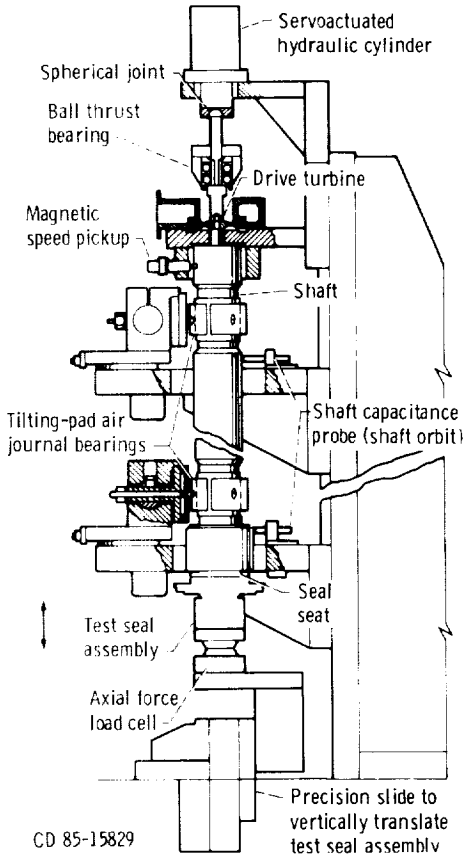

Figure 1.—Seal test apparatus.

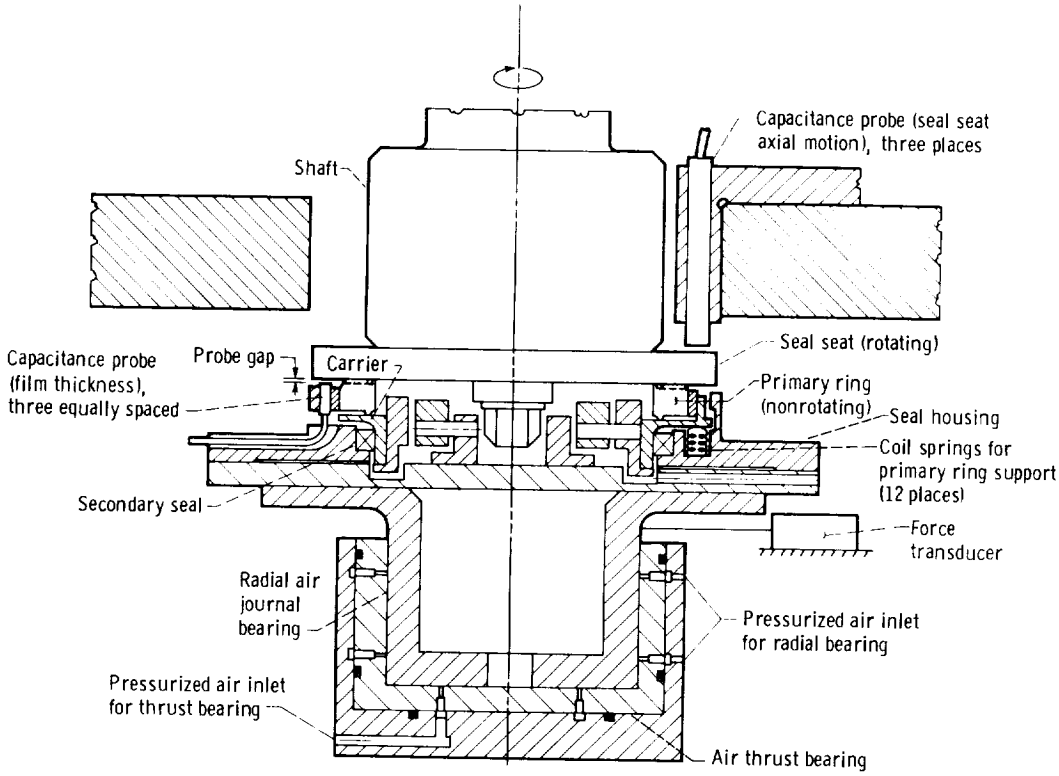

Figure 3.—Schematic of test seal assembly.

to the shaft by a central nut and rotated with the shaft. The primary ring was retained by the carrier, which was suspended on 12 coil springs equally spaced (fig. 3). The equivalent spring rate of the 12 springs was 117 N/cm (67 lb/in.), and the primary ring and carrier together weighed 304 g (0.67 lb). Note that this method of primary ring suspension is typical of face seals, in contrast to the gimbal suspension used in the tests of reference 2.

The seal housing (fig. 3) was floated on radial and thrust air bearings for the purpose of measuring frictional torque between the seal faces. The test seal assembly was mounted on a load cell (fig. 1). This load cell was used to set and monitor the film axial load at the seal faces. The test seal assembly and load cell were mounted on a precision slide (fig. 1). This enabled remote vertical movement of the primary ring away from the seal seat for startup and shutdown and also permitted setting different axial loads at the seal faces while the test was in progress.

The purposes of the servoactuated hydraulic cylinder were to support the shaft and to permit induced axial vibrations of the seal seat under controlled conditions (i.e., controlled amplitude, frequency, and type of seal seat motion). This enabled determination of the film thickness response to axial vibration of the seal seat.

Test Seal Configurations

The two self-acting face seal configurations tested were (1) an inward-pumping spiral-groove seal (fig. 4 and table I) and (2) an outward-pumping spiral-groove seal (fig. 5 and table II). The inward-pumping seal was optimized (i.e., the lift force was maximized for this geometry). References 8 and 9 discuss the optimization of spiral-groove geometry. Note that for both seals the self-acting geometry was machined on the seal seat and the primary ring was a flat surface. The material for both of the seal seats (rotating face) was Monel 502. The material for both of the primary rings was carbon graphite.

Variable-Friction Secondary Seal

To determine the effect of secondary seal friction on the dynamic response of the film thickness in self-acting seals, a variable-friction secondary seal was designed (ref. 10). With this secondary seal the Coulomb damping applied to the primary ring carrier could be remotely varied by varying the friction force applied to the carrier during the seal experiments. The variable-friction secondary seal concept used (fig. 6) consisted of a secondary seal ring with a radial split line and an inflatable rubber bladder. Inflating the bladder with air through the air pressure inlet tube changed the radial load that the secondary seal ring imposed on the primary ring carrier. This changed the axial friction force applied to the carrier. The secondary seal ring material was 4130 steel, and the primary ring carrier was Invar 36 FM chromium plated at the contact region of the seal ring.

Secondary-seal bladder inflation pressure was calibrated versus secondary-seal axial static friction force (fig. 7) by

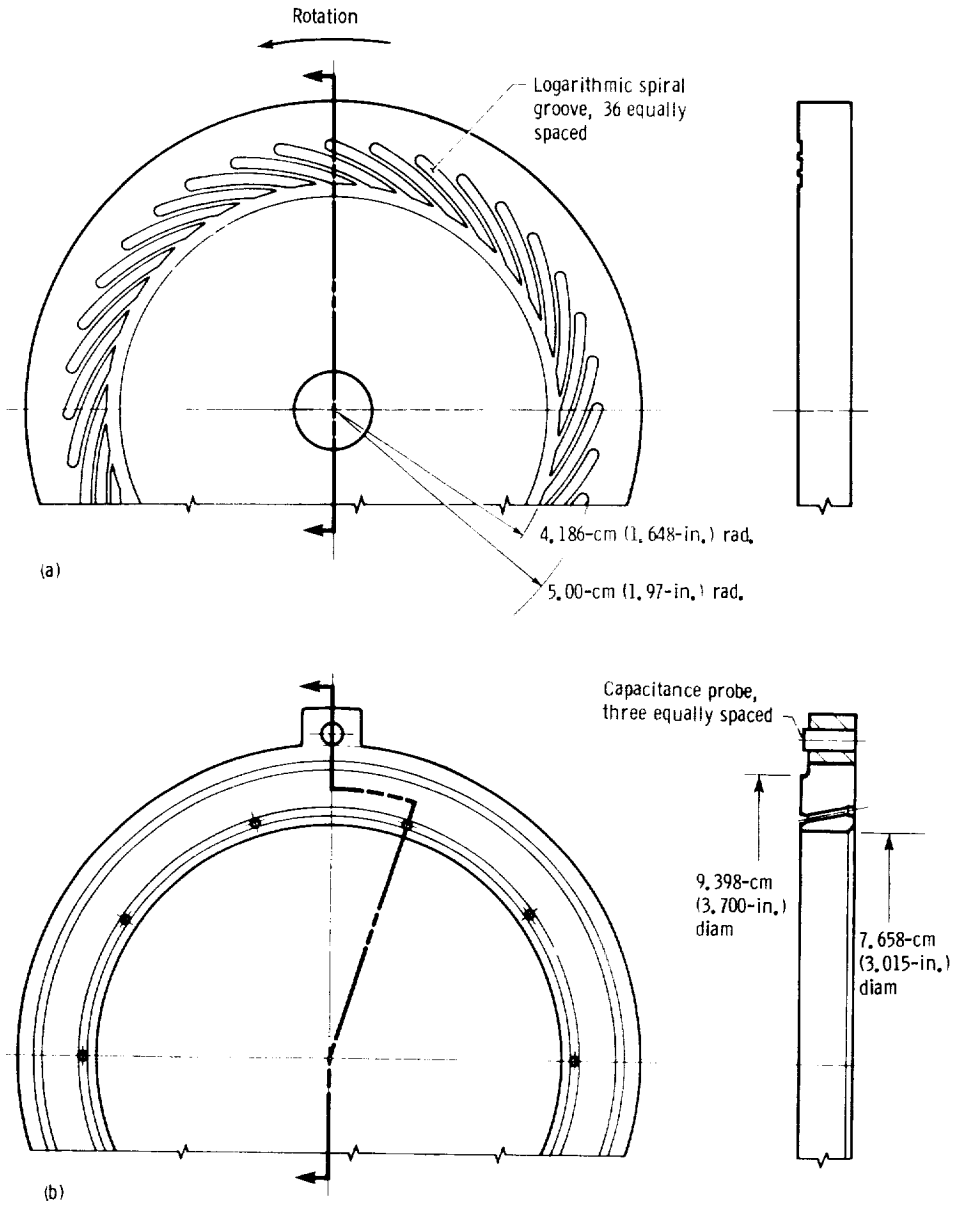

(a) Seat.
(b) Primary ring.

Figure 4.—Details of inward-pumping spiral-groove seal.

TABLE I.—DIMENSIONS OF INWARD-PUMPING SPIRAL-GROOVE SEAL

Outside radius, cm (in.)	4.699 (1.850)
Inside radius, cm (in.)	4.084 (1.608)
Seal band radius, cm (in.)	4.186 (1.648)
Spiral-groove depth, cm (in.)	0.0015 (0.0006)
Groove width (measured circumferentially), cm (in.)	0.549 (0.216)
Land width (measured circumferentially), cm (in.)	0.229 (0.090)
Groove-to-land width ratio	2.40
Spiral-groove angle, deg	20

TABLE II.—DIMENSIONS OF OUTWARD-PUMPING SPIRAL-GROOVE SEAL

Outside radius, cm (in.)	4.699 (1.850)
Inside radius, cm (in.)	4.084 (1.608)
Seal band radius, cm (in.)	4.572 (1.800)
Spiral-groove depth, cm (in.)	0.0018 (0.0007)
Groove width (measured circumferentially), cm (in.)	0.455 (0.179)
Land width (measured circumferentially), cm (in.)	0.279 (0.110)
Groove-to-land width ratio	1.63
Spiral-groove angle, deg	20

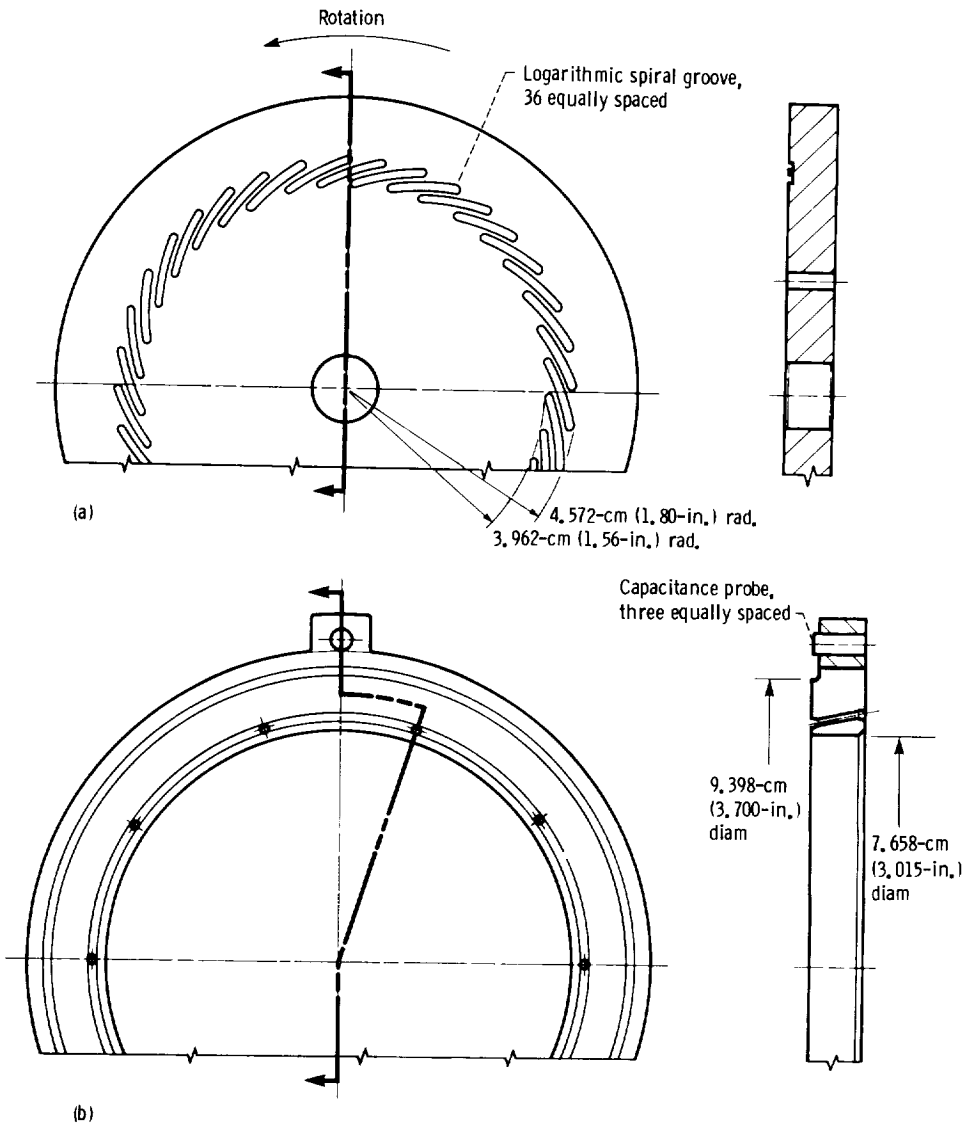

(a) Seat.
(b) Primary ring.

Figure 5.—Details of outward-pumping spiral-groove seal.

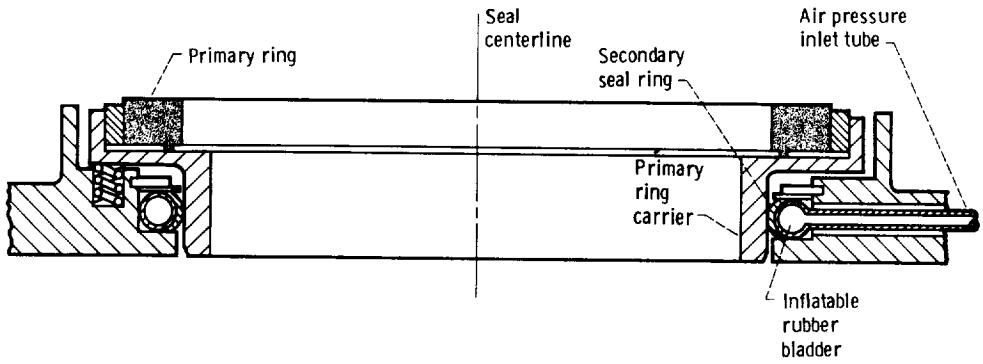

Figure 6.—Schematic showing variable-friction secondary seal.

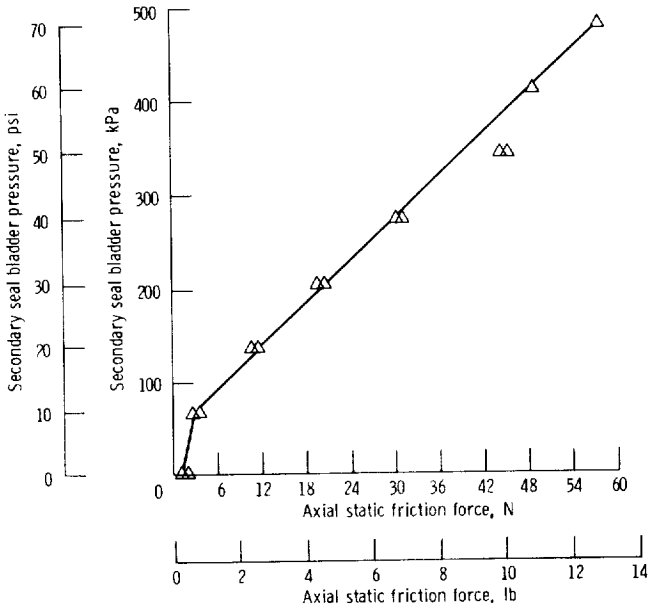

Figure 7.—Variable-friction secondary seal calibration curve for axial friction force.

setting a given secondary-seal bladder inflation pressure and then placing deadweights on the primary ring and noting when motion took place. The calibration was done for bladder pressures from zero to 483 kPa (70 psig). Note that at zero bladder pressure the static axial friction was 0.89 to 1.78 N (0.2 to 0.4 lb). This was due to a slight compression of the secondary seal ring by the bladder so that the seal ring was not loose at zero inflation pressure. The range of axial friction and the sliding characteristics can be altered by selectively choosing the seal ring material or its surface coating.

Segmented Secondary Seal

The segmented secondary seal was a conventional segmented circumferential seal with three segments. The material was carbon graphite, which mated to the chromium-plated Invar carrier. The axial static friction force for this seal, 0.9 N (0.2 lb), was measured in the same manner as for the variable-friction secondary seal.

Instrumentation

The film thickness between the seal seat and the primary ring was directly measured by three capacitance probes mounted as shown in figures 2 and 3. These probes (fig. 8) were equally spaced around the circumference and located at a radius of 5.23 cm (2.06 in.). The initial gap between the probes and the seal seat was 76 μm (3 mils) when the seal seat was contacting the primary ring. The linear measuring range of these probes was 0 to 250 μm (0 to 10 mils). The three probes were cemented into the primary ring retainer (figs. 2 and 3) and individually calibrated in a calibration

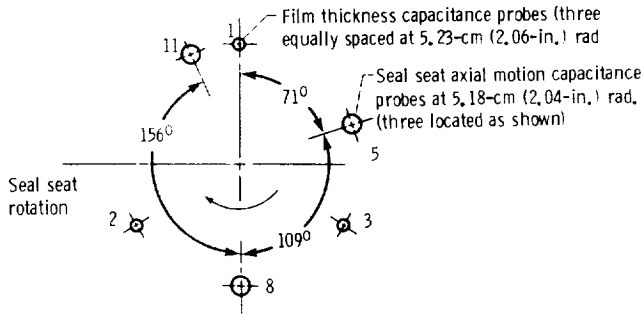

Figure 8.—Capacitance probe locations for film thickness and seal seat axial motion. (View looking down.)

fixture. The resolution was 0.025 μm (1 μin.), and the accuracy was estimated to be ± 0.5 μm (20 μin.).

The seal seat axial motion was measured by three capacitance probes facing the top surface of the seal seat (fig. 3). These probes were located as shown in figure 8. The unequal circumferential spacing was due to rig space limitations. The linear measuring range of these probes was 0 to 250 μm (0 to 10 mils). Each probe was individually calibrated in a calibration fixture and installed in the rig. The resolution was 0.025 μm (1 μin.), and the accuracy was estimated to be ± 0.5 μm (20 μin.).

The shaft radial motion at each air journal bearing was monitored by two capacitance probes (fig. 1) facing the shaft at each bearing location and mounted normal to each other. Shaft speed was sensed by a magnetic speed pickup and automatically controlled to hold a given speed. The automatic control system varied turbine drive air pressure to maintain the desired speed. A force transducer was mounted to the gimbal base, which was floated on air bearings (fig. 3), such that the transducer measured the tangential force between the gimbal base and ground. This arrangement provided accurate and sensitive measurement of torque at the seal face for the purpose of detecting seal face rubs during the tests. The force transducer, which was calibrated in the rig assembly by using calibrated weights, measured tangential force at a radius of 34.9 mm (1.375 in.). The resolution was 0.004 N (0.001 lb), and the accuracy was estimated to be ± 0.013 N (0.003 lb).

Data Acquisition System

The capacitance probes, which measured film thickness, seal seat axial motion, and shaft orbit, were fed to capacitance probe amplifiers. The output signal from these amplifiers was proportional to the probe gaps. The frequency response of this system was -3 dB at 5 kHz. This signal was input to a waveform analyzer, where the data were digitized and stored on diskettes. The sampling rate (20 000 Hz) was well above the highest frequency of 1500 Hz measured during the tests. The waveform analyzer could store up to eight channels of data taken simultaneously (i.e., data for all input channels were

recorded at the same instant). The signals for the seal frictional torque and axial load were also sent to the waveform analyzer, digitized, and stored on diskettes. The dynamic data were plotted as a function of time by using plotting routines in the waveform analyzer. The waveform analyzer could also perform fast Fourier transforms (FFT's) of the data signals.

Procedure

The primary rings and seal seats were lapped flat to within three helium light bands before assembly into the test rig. The spiral-groove depths were within 2.5 μm (0.1 mil) of their nominal values. The three capacitance probes that measured film thickness had an initial gap of approximately 76 μm (3 mils) when the gap at the seal faces was zero (zero film thickness). The gap for the three seal seat axial motion probes was approximately 50 μm (2 mils) when the seal faces were contacting. Amplifiers for all instrumentation were set for zero output with the seal faces firmly contacting. Before the turbine drive was started, the seal faces were separated by remotely actuating the slide (fig. 1) to lower the test seal assembly away from the seal seat. The turbine drive was then started and the shaft was accelerated to 14 000 rpm. The test seal assembly was then raised by remotely actuating the slide until the axial force load cell indicated the desired film axial load.

The torquemeter was used as an indicator of impending contact of the seal faces since the torque would rise rapidly in this situation. Once the seal was operating stably, as indicated by the torquemeter, the shaft speed was set to the desired value and allowed to stabilize.

Two types of tests were run: steady seal seat mode and sinusoidal seal seat mode. Details of these modes are discussed later. In the steady mode the digitized data were recorded on diskettes after the axial force was set and conditions were stable. In the sinusoidal mode the servoactuated hydraulic cylinder control system was turned on and set to the desired amplitude and frequency. This caused the seal seat to vibrate axially at the set amplitude and frequency in a near-sinusoidal pattern (the waveform was not a perfect sinusoid because of servosystem limitations). Once the system was stable, the digitized data were recorded on diskettes as functions of time for later evaluation. The data recorded were film thickness (three probes), seal seat axial motion (three probes), seal frictional torque, and film axial load.

Upon completion of the tests the test seal assembly was lowered away from the seal seat by remotely actuating the slide, and the shaft was allowed to coast to a stop.

Discussion of Results

A series of tests were conducted on two spiral-groove face seal configurations

(1) To determine the dynamic response of the film thickness to axial seal seat vibrations

(2) To determine the effect of secondary-seal friction on the dynamic performance of self-acting spiral-groove face seals

(3) To determine the dynamic response of the film thickness to a skewed seal seat

The test conditions are given in the Introduction. The tests were performed with ambient air to minimize seal distortions that could result from elevated temperatures and pressures.

Table III shows a matrix of seal types and test variables. The checkmarks indicate the combinations that were tested. Four seal seat axial motion modes are shown in the table. The steady mode with true seal seat is shown in figure 9(a). The

TABLE III.—SPIRAL-GROOVE SEAL TEST CONFIGURATIONS

Seal seat axial motion mode	Inward-pumping spiral groove			Outward-pumping spiral groove (segmented secondary seal)
	Segmented secondary seal	No secondary seal	Variable-friction secondary seal	
Steady (true seal seat)[a]	✓	✓	✓	✓
Sinusoidal (true seal seat)[b]	✓	✓	✓	✓
Steady (skewed seal seat)[c]				✓
Sinusoidal (skewed seal seat)[c]				✓

[a]Plane of seal seat normal to rotor axis of rotation.
[b]Sinusoidal seal seat axial motion; 50-μm (2-mil) amplitude at 100 Hz.
[c]Plane of seal seat skewed 0.028° with respect to rotor axis of rotation.

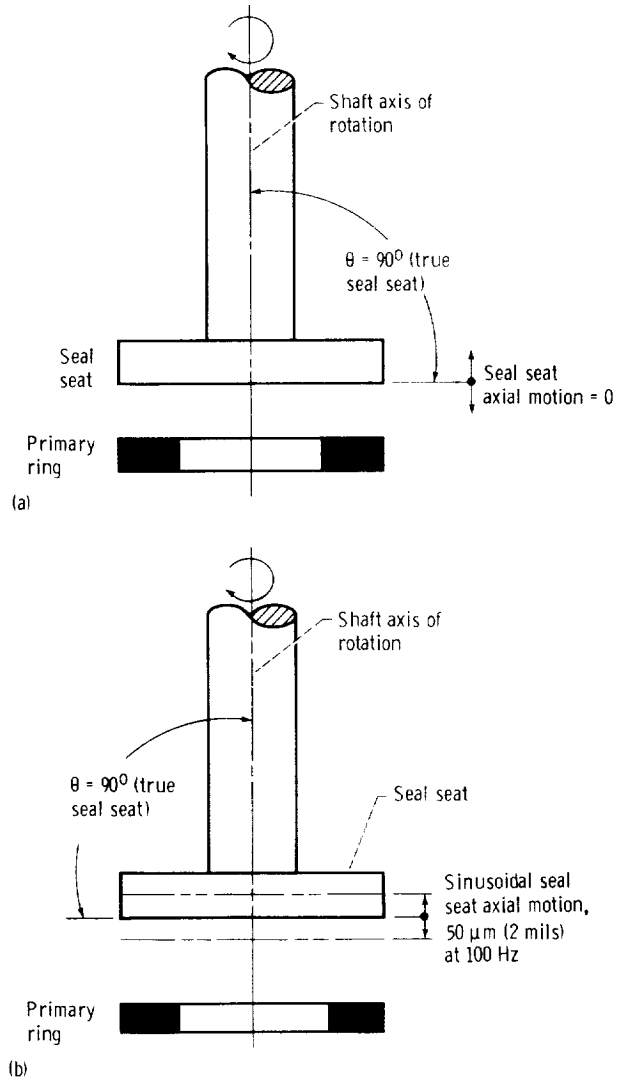

(a) Steady seal seat mode with true seal seat.
(b) Sinusoidal seal seat mode with true seal seat.

Figure 9.—Schematic showing seal seat vibrational modes for true seal seat.

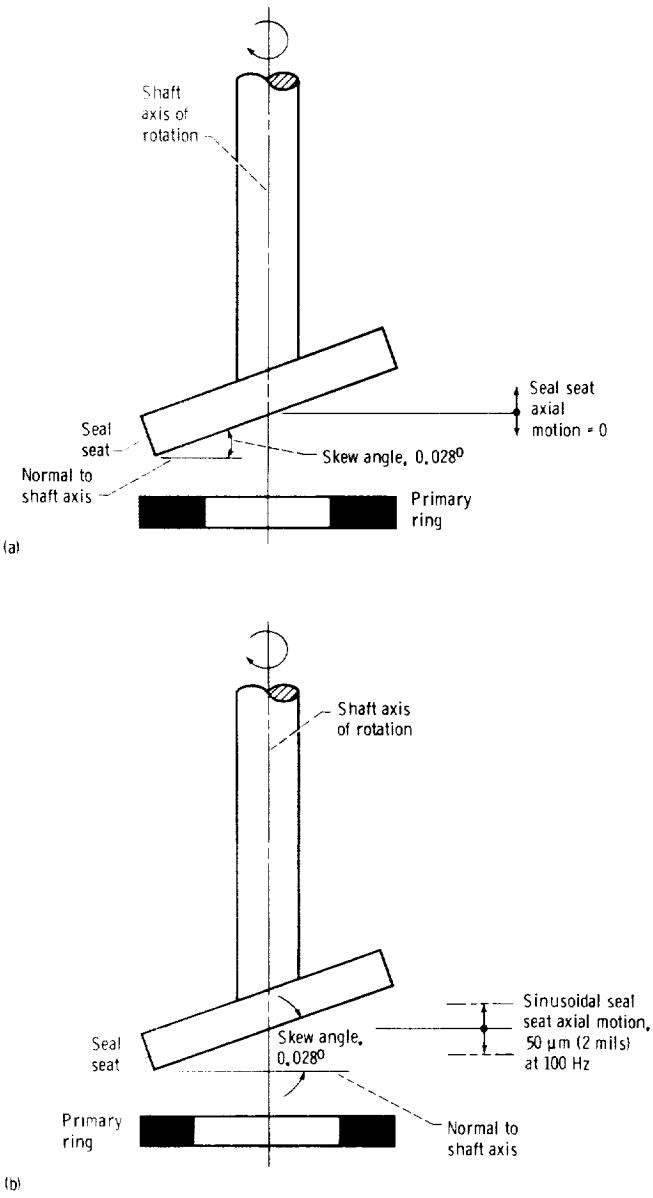

(a) Steady seal seat mode with skewed seal seat.
(b) Sinusoidal seal seat mode with skewed seal seat.

Figure 10.—Schematic showing seal seat vibrational modes for skewed seal seat. (Skew angles are highly exaggerated.)

figure indicates that the seal seat has no axial oscillation and the plane of the seal seat face is normal to the shaft axis of rotation. This mode established baseline data. The sinusoidal mode with true seal seat is shown in figure 9(b). The sinusoidal axial motion shown in the figure is an induced axial oscillation of the seal seat with an amplitude of 50 μm (2 mils) at 100 Hz. Note that the angle between the plane of the true seal seat and the rotor axis was 90°. The remaining two modes were the same as the first two except that the plane of the seal seat was skewed 0.028° (50 μm, or 2 mils, across the seal face) with respect to the rotor axis of rotation (fig. 10). For the steady mode the skewed seat produced a swashing type of seal seat motion; for the sinusoidal mode it produced a swashing motion superimposed on the sinusoidal translation. These motions will be described later. The sinusoidal mode and skewed seal seat were used to determine the film thickness response to these types of seal seat motions.

Three secondary-seal configurations were tested (table III) to determine the effect of secondary-seal friction on film vibrations. These were a conventional carbon circumferential seal with three segments, no secondary seal, and a variable-friction secondary seal (discussed previously). A segmented circumferential seal is a ring seal composed of several circular segments retained in place by a garter spring around the circumference.

Steady Seal Seat Mode (Inward-Pumping Spiral-Groove Seal)

Film thickness as a function of time was plotted for the inward-pumping spiral-groove seal (fig. 4, table I) at 7000 and 14 000 rpm. Typical traces for the steady seal seat mode with true seal seat are shown in figures 11 to 13. Figure 11 is for the carbon segmented circumferential seal, figure 12 is for the variable-friction secondary seal (no bladder pressure), and figure 13 is for no secondary seal. These figures represent baseline data to which the dynamic data were compared. Traces for the inward-pumping seal at 7000 and 14 000 rpm are shown because of their grossly different film thickness patterns. Grossly different film thickness patterns depending on speed were also reported in reference 2. In the tests of reference 2 the primary ring was supported on a gimbal mount in contrast to the coil spring support of these tests (see the section Seal Test Apparatus). Therefore this effect was not

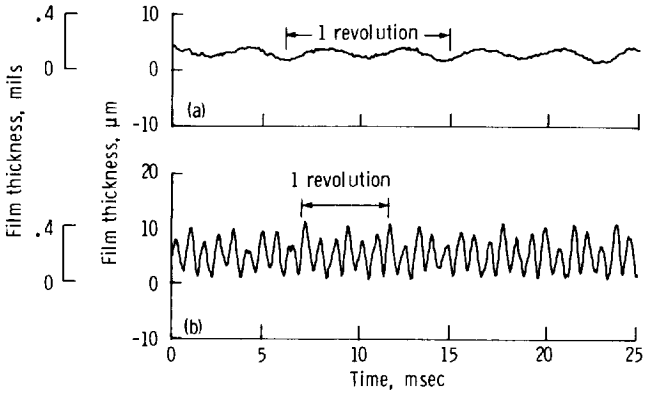

(a) Shaft speed, 7000 rpm.
(b) Shaft speed, 14 000 rpm

Figure 11.—Film thickness as function of time (probe 1) for inward-pumping spiral-groove seal, segmented secondary seal, and steady seal seat mode.

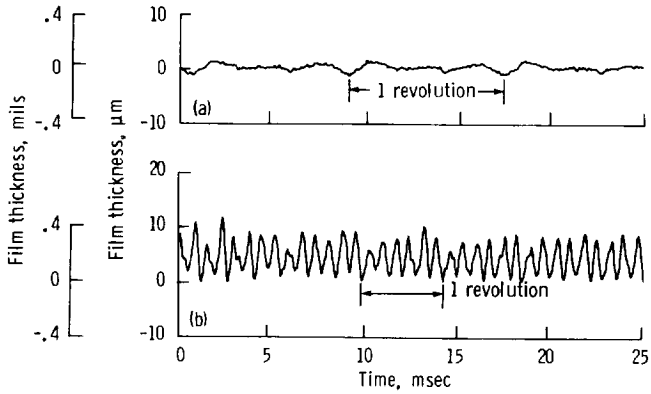

(a) Shaft speed, 7000 rpm.
(b) Shaft speed, 14 000 rpm.

Figure 12.—Film thickness as function of time (probe 1) for inward-pumping spiral-groove seal, variable-friction secondary seal (no bladder pressure), and steady seal seat mode.

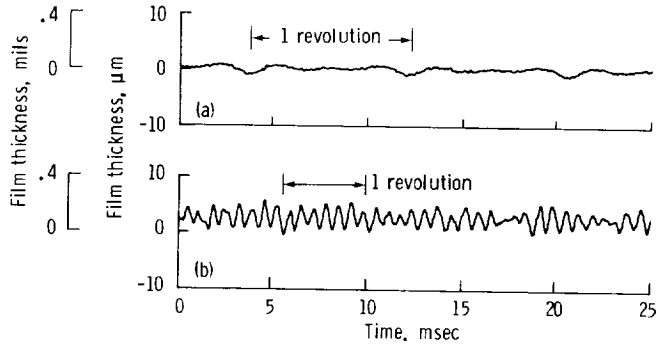

(a) Shaft speed, 7000 rpm.
(b) Shaft speed, 14 000 rpm.

Figure 13.—Film thickness as function of time (probe 1) for inward-pumping spiral-groove seal, no secondary seal, and steady seal seat mode.

due to the primary ring support system and appeared to be peculiar to the inward-pumping seal since it was not observed in the outward-pumping seal. The 7000-rpm traces were typical for speeds below approximately 10 000 rpm, and the 14 000-rpm traces were typical for speeds above 10 000 rpm. Figures 14 to 16, the fast Fourier transforms (FFT's) of figures 11 to 13, respectively, indicate the active frequencies for each film thickness trace. The FFT's indicate very small synchronous response and show the film thickness frequency to be twice synchronous for the 7000-rpm case and approximately six times synchronous for the 14 000-rpm case. The configurations with a variable-friction secondary seal and no secondary seal (figs. 15(a) and 16(a)) showed a response at three times synchronous as well as at twice synchronous. Although film thickness was measured at three circumferential locations (fig. 8), only the probe 1 trace is shown because the three probes had similar traces except for phase. Data from all three probes, however, were used to calculate primary ring

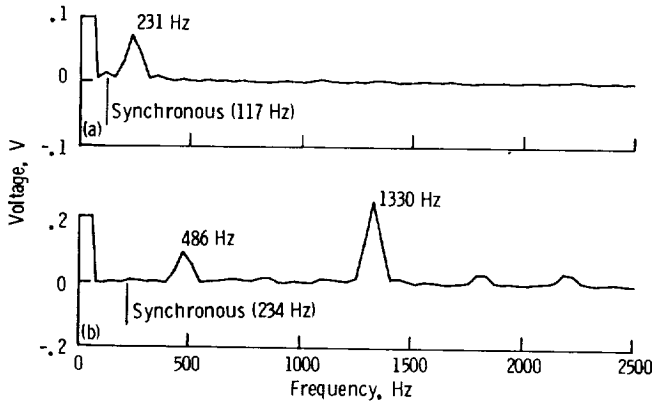

(a) Shaft speed, 7000 rpm.
(b) Shaft speed, 14 000 rpm.

Figure 14.—Fast Fourier transform of film thickness (probe 1) for inward-pumping spiral-groove seal, segmented secondary seal, and steady seal seat mode.

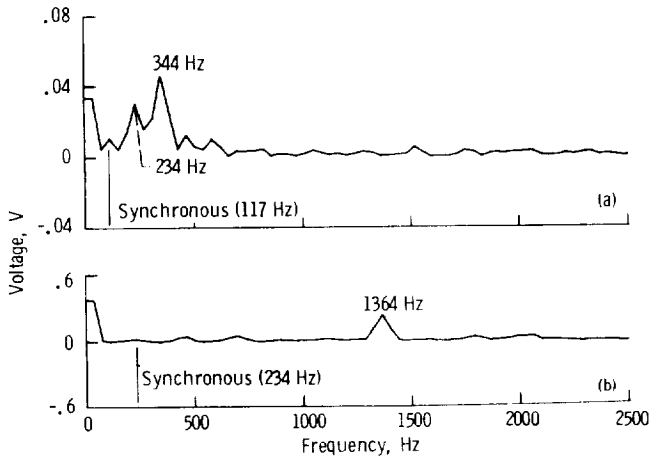

(a) Shaft speed, 7000 rpm.
(b) Shaft speed, 14 000 rpm.

Figure 15.—Fast Fourier transform of film thickness (probe 1) for inward-pumping spiral-groove seal, variable-friction secondary seal (no bladder pressure), and steady seal seat mode.

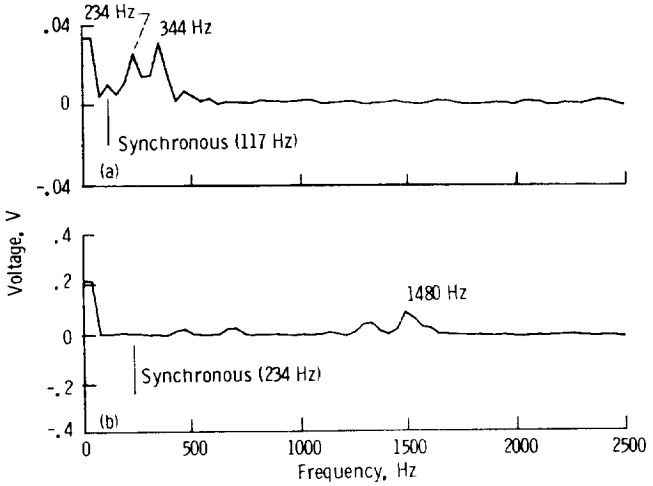

(a) Shaft speed, 7000 rpm.
(b) Shaft speed, 14 000 rpm.

Figure 16.—Fast Fourier transform of film thickness (probe 1) for inward-pumping spiral-groove seal, no secondary seal, and steady seal seat mode.

tilt angles (angle between seal seat face and primary ring face) as a function of time. This is discussed in a later section.

The axial motion of the seal seat was measured by probes 5, 8, and 11 for the steady mode with true seal seat (fig. 17). This trace is typical of all steady-mode configurations with true seal seats. The probes indicated an axial runout of approximately 5 μm (0.2 mil) for this mode. This runout was due to shaft wobble and small assembly and fabrication misalignment. Ideally the runout should be zero (perfectly straight lines in the traces). The FFT of probe 5 indicated no response at any frequency.

To get a graphical indication of the angular displacement, or rocking motion, of the primary ring, it was necessary to plot the angle between the plane of the seal seat and the plane

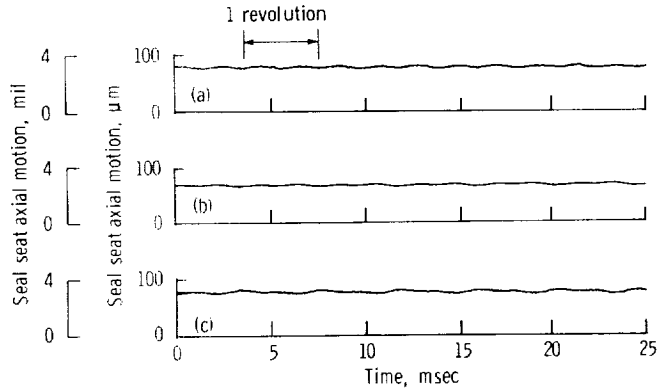

(a) Probe 5.
(b) Probe 8.
(c) Probe 11.

Figure 17.—Seal seat axial motion for steady seal seat mode and 14 000-rpm shaft speed.

of the primary ring as a function of time. This is called the tilt angle and is defined in figure 18. The tilt angles β_x and β_y, about the x and y axes, respectively, were computed from the digitized experimental film thickness data from probes 1 to 3 for each time sample.

The tilt angles β_x and β_y were plotted as a function of time for the inward-pumping seal with a segmented secondary seal for the steady mode at 7000-rpm shaft speed (figs. 19(a) and (b)). The resultant tilt angle (fig. 19(c)) was the vector sum of β_x and β_y and indicated the resultant magnitude of the tilt angle. For 7000 rpm the tilt angle had a rather clean, almost sinusoidal, pattern at a frequency of twice synchronous speed (fig. 19). The tilt angle about the x axis (fig. 19(a)) was nearly symmetrical about zero, while the angle about the y axis (fig. 19(b)) was biased toward the negative.

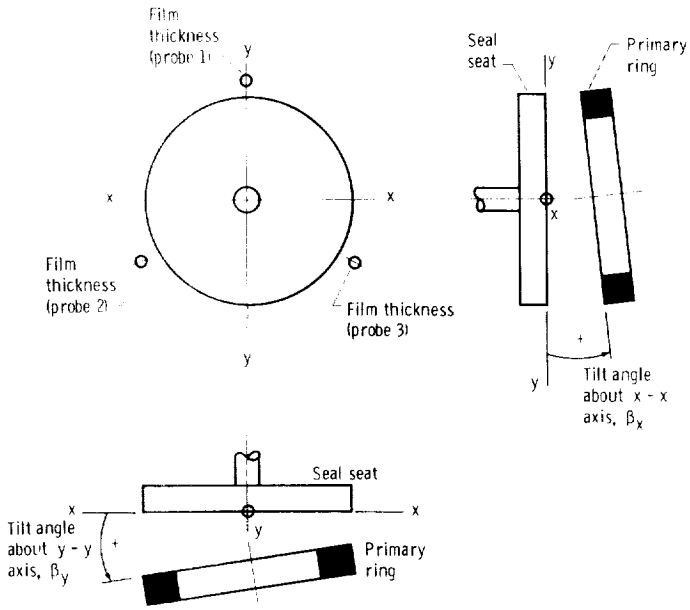

Figure 18.—Schematic showing definition of tilt angle.

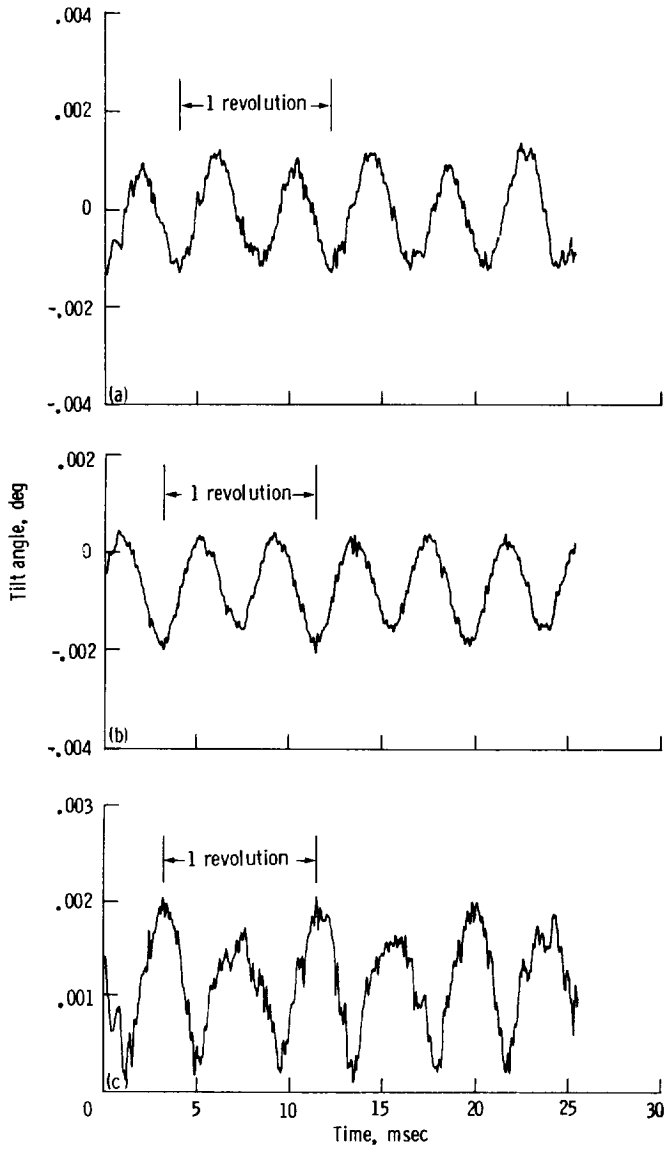

(a) Tilt angle about x axis (β_x).
(b) Tilt angle about y axis (β_y).
(c) Resultant tilt angle.

Figure 19.—Tilt angle as function of time for inward-pumping spiral-groove seal, segmented secondary seal, steady seal seat mode, and 7000-rpm shaft speed.

The tilt angle at 14 000 rpm for the segmented secondary seal (fig. 20), unlike the 7000-rpm case (fig. 19), had a complex waveform. There were approximately two direction reversals per shaft revolution for the x axis (fig. 20(a)) and two for the y axis (fig. 20(b)). The resultant tilt angle excursion (fig. 20(c)) was approximately 0.004° as compared with 0.002° for the 7000-rpm case (fig. 19(c)). Tilt angles were generated for the configurations with a variable-friction

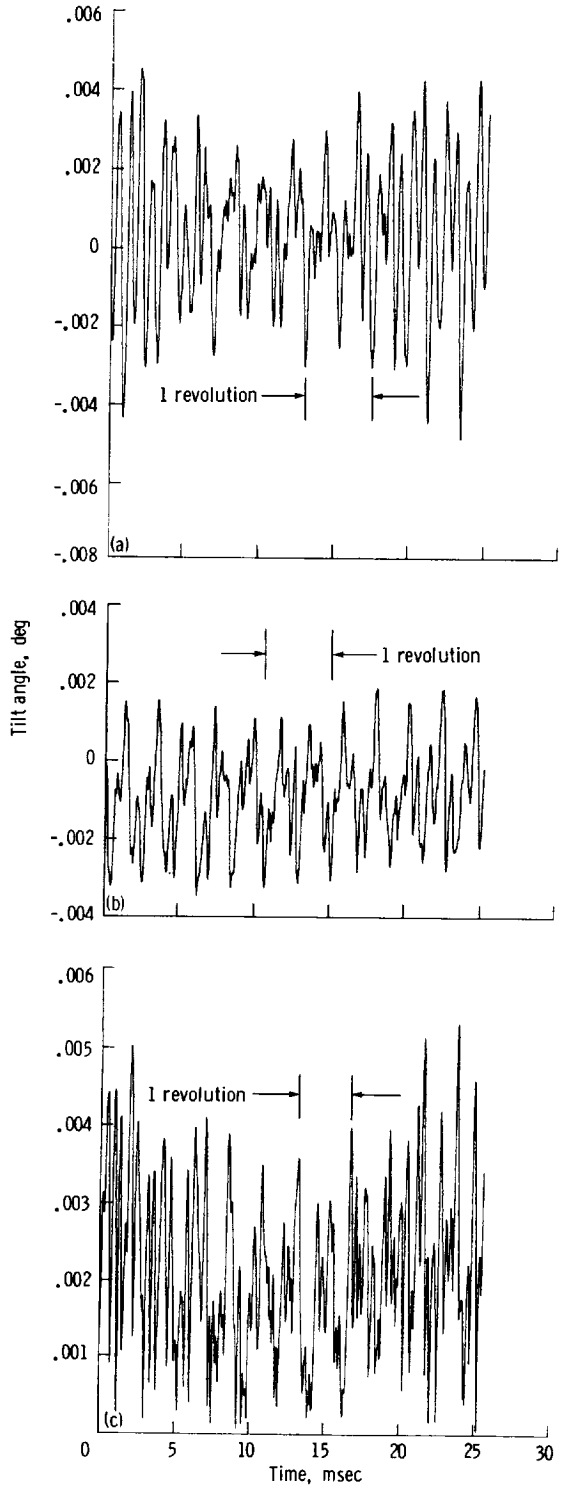

(a) Tilt angle about x axis (β_x).
(b) Tilt angle about y axis (β_y).
(c) Resultant tilt angle.

Figure 20.—Tilt angle as function of time for inward-pumping spiral-groove seal, segmented secondary seal, steady seal seat mode, and 14 000-rpm shaft speed.

secondary seal and no secondary seal and were found to be similar to the traces for the segmented secondary seal.

Since three different secondary seal configurations are shown in figures 11 to 13 these figures can be used to evaluate the effect of secondary seal friction on film vibration. The traces in figures 11 and 12 are very similar, indicating that the difference in friction and geometry between the segmented secondary seal and the variable-friction secondary seal had no effect on the film vibration pattern for the steady mode. The static friction between the secondary seal and the carrier was 0.9 N (0.2 lb) for the segmented secondary seal and 1.4 N (0.3 lb) for the variable-friction secondary seal. Note that the secondary seal static friction measurement is described in the section Variable-Friction Secondary Seal. The film thickness trace for the configuration with no secondary seal (fig. 13) indicated that the film vibration amplitude (4 μm; 0.16 mil) was less than for the other two configurations (9 μm; 0.35 mil). Thus minimizing secondary seal friction reduced film vibration at the axial film load (73 N; 16.4 lb) and speed tested in this case. For higher axial film loads and higher speeds, however, higher friction loads were required to maintain stability (as discussed later). The vibratory frequency for all three secondary seal configurations was nearly the same (approx. six times synchronous).

Sinusoidal Seal Seat Mode (Inward-Pumping Spiral-Groove Seal)

The seal seat motion for the sinusoidal seal seat mode (fig. 21) was not purely sinusoidal because of the limits of the servovalve control system. The motion was a pure axial translation of the seal seat without wobble because the three traces (probes 5, 8, and 11) are in phase. Phase differences between these three probes would indicate a complex wobbling motion of the seal seat. The amplitude of the seal seat was 50 μm (2 mils) at 100 Hz for this mode. The traces shown in figure 21 are typical for all of the sinusoidal seal seat mode tests. The FFT's for these traces were flat and indicated a response only at the seal seat oscillating frequency of 100 Hz.

The film thickness response (probe 1) for the segmented secondary seal at 7000 rpm was the same for the steady and sinusoidal seal seat modes (fig. 22). The primary ring tracked the high amplitudes of the seal seat quite well at 100 Hz. The film thickness variation was only 2.7 μm (0.1 mil) peak to peak when the seal seat amplitude was 100 μm (4 mils) peak to peak. Perfect tracking would be indicated by a straight line in these traces (i.e., no change in film thickness as a function of time). The FFT's of the film thickness for both the steady and sinusoidal seal seat modes were virtually the same and indicated a response at twice synchronous (fig. 14(a)).

Tests were also run at various seal seat amplitudes to 50 μm (2 mils) at frequencies of 10 to 50 Hz to determine the effect of frequency on the film thickness response. These tests showed the response to be the same as that shown in figure 22 for all frequencies. This seal appeared to have excellent tracking ability to pure axial translations of the seal seat for

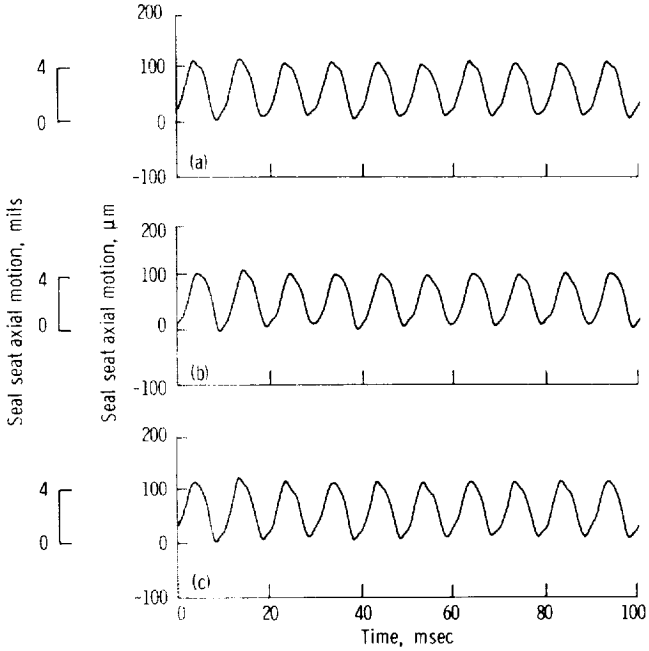

(a) Probe 5.
(b) Probe 8.
(c) Probe 11.

Figure 21.—Seal seat axial motion for sinusoidal seal seat mode (50-μm (2-mil) amplitude at 100 Hz).

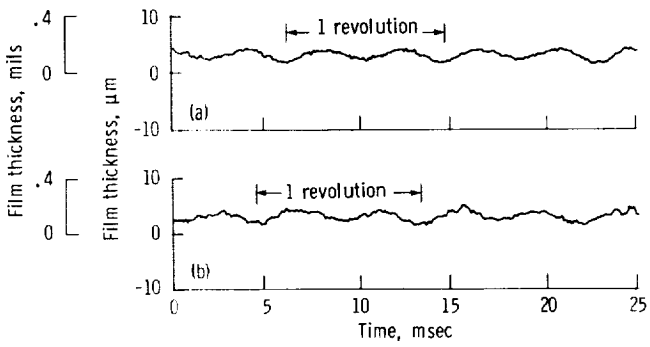

(a) Steady seal seat mode.
(b) Sinusoidal seal seat mode. Amplitude, 50 μm (2 mils); frequency, 100 Hz.

Figure 22.—Film thickness as function of time (probe 1) for inward-pumping spiral-groove seal, segmented secondary seal, and 7000-rpm shaft speed.

frequencies at least to 100 Hz. Note that 100 Hz was a limit of the servovalve control system and does not suggest that the seal would not track well above this frequency.

During these test runs the frictional torque between the seal faces was monitored as discussed previously. The torque was stable with no spikes, indicating that there were no rubs for either seal seat mode during these tests. The seal frictional torque was 1.58 N-cm (0.14 in.-lb) for both modes.

The film thickness response (probe 1) was compared for the steady and sinusoidal seal seat modes at 14 000 rpm (fig. 23). All other parameters were the same as for the 7000-rpm case (fig. 22). The film thickness amplitudes were somewhat lower

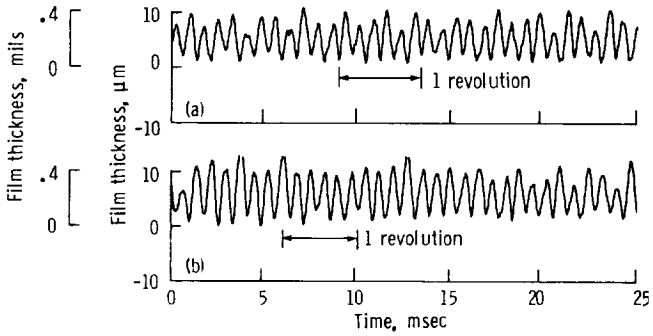

(a) Steady seal seat mode.
(b) Sinusoidal seal seat mode. Amplitude, 50 μm (2 mils); frequency, 100 Hz.

Figure 23.—Film thickness as function of time (probe 1) for inward-pumping spiral-groove seal, segmented secondary seal, and 14 000-rpm shaft speed.

for the steady mode (fig. 23(a)) than for the sinusoidal mode (fig. 23(b)), and the frequency of the film vibration was approximately the same (six times synchronous for both cases). The FFT's for both cases were the same and indicated a response at twice and six times synchronous (fig. 14(b)). Thus the sinusoidal seal seat motion had no effect on the tracking ability of the seal. The response shown in figure 23(b) is typical for all sinusoidal seal seat mode frequencies within the test range (to 100 Hz). The seal frictional torque was 2.37 N-cm (0.21 in.-lb) for both modes and was steady with no spikes, an indication that the seal faces did not rub.

The film thickness response to the steady and sinusoidal seal seat modes at 14 000 rpm was plotted for the variable-friction secondary seal with zero bladder inflation pressure (fig. 24). The static friction between the carrier and the secondary seal was 1.4 N (0.3 lb). The film thickness amplitude for the steady mode (fig. 24(a)) was again somewhat less than for the sinusoidal mode, and both had frequencies of approximately six times synchronous. Thus the sinusoidal seal seat motion had no effect on the tracking ability of the seal for this case. The waveform was very similar to that for the segmented secondary seal (fig. 23) and indicated that changing the

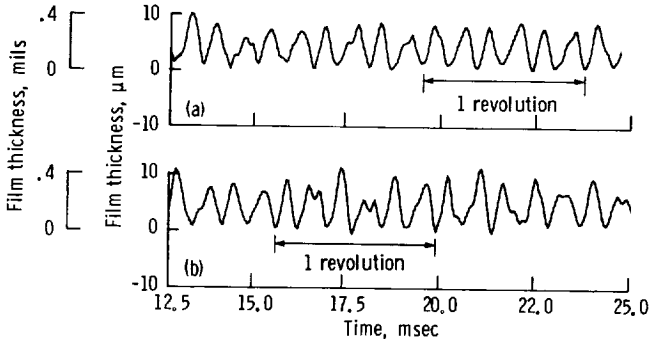

(a) Steady seal seat mode.
(b) Sinusoidal seal seat mode. Amplitude, 50 μm (2 mils); frequency, 100 Hz.

Figure 24.—Film thickness as function of time (probe 1) for inward-pumping spiral-groove seal, variable-friction secondary seal (no bladder pressure), and 14 000-rpm shaft speed.

secondary seal had little effect on the film thickness response for zero bladder inflation pressure. (See discussion on variable-friction secondary seal.) The film thickness response to the sinusoidal seal seat motion was the same for all frequencies within the test range (to 100 Hz). The FFT's for these cases were the same and indicated a response at six times synchronous (fig. 15(b)). The seal frictional torque was stable at 2.82 N-cm (0.25 in.-lb) without any spikes, an indication that the seal faces did not rub.

The film thickness response for no secondary seal at 14 000 rpm was determined for the steady and sinusoidal seal seat modes (fig. 25). The film thickness trace for the steady mode (fig. 25(a)) showed a film vibration of six times synchronous but with a decaying amplitude. This was not seen for the sinusoidal mode (fig. 25(b)) or for the cases discussed previously. The film thickness response for the sinusoidal mode showed a frequency approximately six times synchronous, quite similar to the other types of secondary seal cases except that the amplitude was less. The FFT's for these cases were similar and indicated responses at approximately six times synchronous (fig. 16(b)). The seal frictional torque was 2.03 N-cm (0.18 in.-lb) and stable, indicating no seal rubs during this test.

Film thickness responses for the variable-friction secondary seal were compared at zero and 276-kPa (40-psig) bladder inflation pressure (fig. 26). (See discussion on variable-friction secondary seal.) The static friction between the carrier and the secondary seal was 0.9 N (0.2 lb) at zero bladder pressure (fig. 26(a)) and 31.1 N (7 lb) at 276 kPa (40 psig) (fig. 26(b)). These data are for the steady seal seat mode at 14 000 rpm. The film thickness traces in figures 26(a) and (b) look much the same. The FFT's for these cases indicated response at six times synchronous (fig. 15(b)). The seal frictional torque for the 276-kPa (40-psig) case was 5.90 N-cm (0.52 in.-lb), indicating possible light uniform rubbing of the seal faces. The torque, however, was stable with no spikes.

When the secondary seal bladder inflation pressure was set at 345 kPa (50 psig), which produced 40-N (9-lb) static friction force between the seal carrier and the secondary seal, the seal

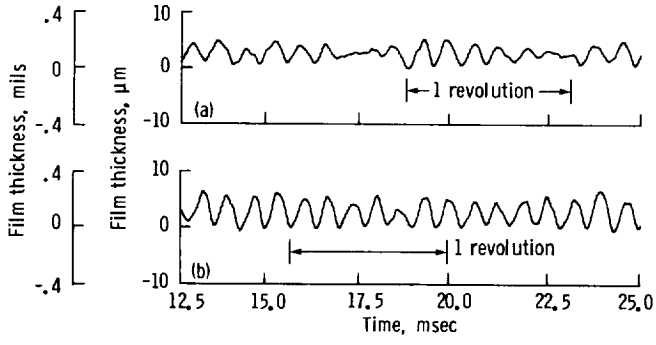

(a) Steady seal seat mode.
(b) Sinusoidal seal seat mode. Amplitude, 50 μm (2 mils); frequency, 100 Hz.

Figure 25.—Film thickness as function of time (probe 1) for inward-pumping spiral-groove seal, no secondary seal, and 14 000-rpm shaft speed.

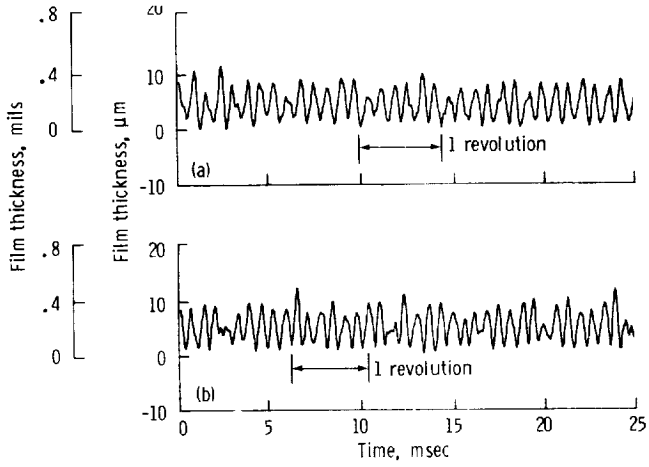

(a) Secondary seal bladder pressure, zero.
(b) Secondary seal bladder pressure, 276 kPa (40 psig).

Figure 26.—Film thickness as function of time (probe 1) for inward-pumping spiral-groove seal, variable-friction secondary seal, steady seal seat mode, and 14 000-rpm shaft speed.

frictional torque became erratic and heavy rubbing of the seal faces occurred. Thus the onset of instability took place when static friction levels were approximately 31 to 40 N (7 to 9 lb) for this seal.

The effect of changing the secondary seal friction was seen in the film axial load: as the secondary seal friction was increased, the film axial load also increased. The film axial load was reset to 73 N (16.4 lb) by remotely lowering the primary ring assembly (see discussion of film axial load measurement).

Tests were run on the inward-pumping seal for the sinusoidal seal seat mode for an amplitude of 60 μm (2.5 mils) at 50 Hz and speeds from 14 000 to 20 000 rpm to determine the film thickness response for speeds above 14 000 rpm. The tests were run with the segmented secondary seal. There was no change in film thickness response over this speed range. Similarly tests run for the sinusoidal mode for 60-μm (2.5-mil) amplitude at 100 Hz and 20 000 rpm and also at 100-μm (4-mil) amplitude at 50 Hz and 20 000 rpm indicated no change in film thickness response. During these tests the seal frictional torque was stable with no spikes, and there was no indication of seal face rubbing. The speed of 20 000 rpm is a rig speed limit and does not indicate a speed limit for the seal.

Tests were also run for both the steady and sinusoidal seal seat modes (50 μm (2 mils) at 100 Hz) at 14 000 rpm for film axial loads to 95.6 N (21.5 lb). The film thickness traces were similar to those for 73 N (16.4 lb) except for the lower average film thickness at the higher loads. The seal frictional torque was stable throughout this load range, and there was no indication of seal face rubbing.

Tests run on the inward-pumping spiral-groove seal with no secondary seal for the steady seal seat mode showed that for speeds above 18 500 rpm with 73-N (16.4-lb) film axial load the seal seat frictional torque became unstable and spiked, indicating heavy seal face rubs above this speed. Also the seal was unstable at 89-N (20-lb) axial force at 20 000 rpm. As discussed previously, the seal with the segmented secondary seal did not display these instabilities at these conditions. This indicates that the axial friction force produced by the segmented secondary seal (1.9 N; 0.2 lb) was necessary at the higher speeds and loads to promote smooth stable operation of this self-acting seal.

Outward-Pumping Spiral-Groove Seal

Tests were run on an outward-pumping spiral-groove seal with a segmented secondary seal (fig. 5; table II). These tests were similar to those for the inward-pumping seal except that the tests were run with a skewed seal seat as well as with the true seal seat (figs. 9 and 10).

The film thickness response for the steady mode and true seal seat for 10 500, 14 000, and 19 800 rpm (fig. 27) represents a baseline response. The seal seat axial motion for this mode is shown in figure 17. The film thickness traces were very similar over this entire speed range and did not display high amplitudes at the higher speeds as did those for the inward-pumping seal (fig. 11). The FFT's for these cases (fig. 28) showed responses at two, three, and four times synchronous for all three speeds. The torque was stable for these cases and was 2.8 N-cm (0.25 in.-lb) for 10 500 rpm, 3.1 N-cm (0.28 in.-lb) for 14 000 rpm, and 3.4 N-cm (0.30 in.-lb) for 19 800 rpm. No seal rubs were observed during these cases.

The film thickness responses to the sinusoidal mode with true seal seat for 10 500 and 19 800 rpm (fig. 29) are very similar to figure 27. This indicates no difference in tracking ability between these two modes. The seal frictional torque

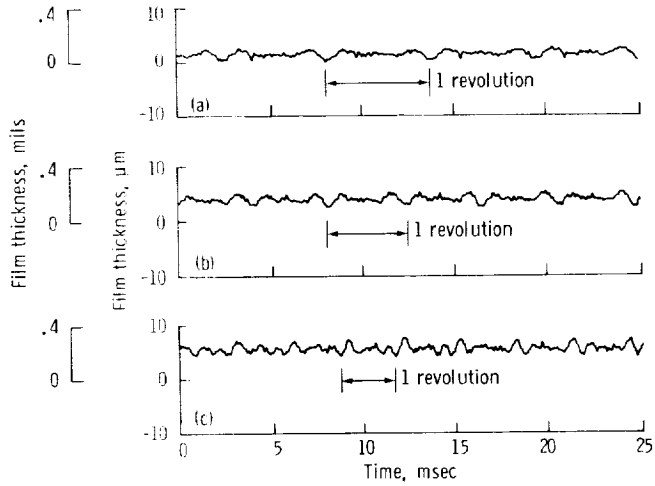

(a) Shaft speed, 10 500 rpm.
(b) Shaft speed, 14 000 rpm.
(c) Shaft speed, 19 800 rpm.

Figure 27.—Film thickness as function of time (probe 1) for outward-pumping spiral-groove seal, segmented secondary seal, steady seal seat mode, and true seal seat.

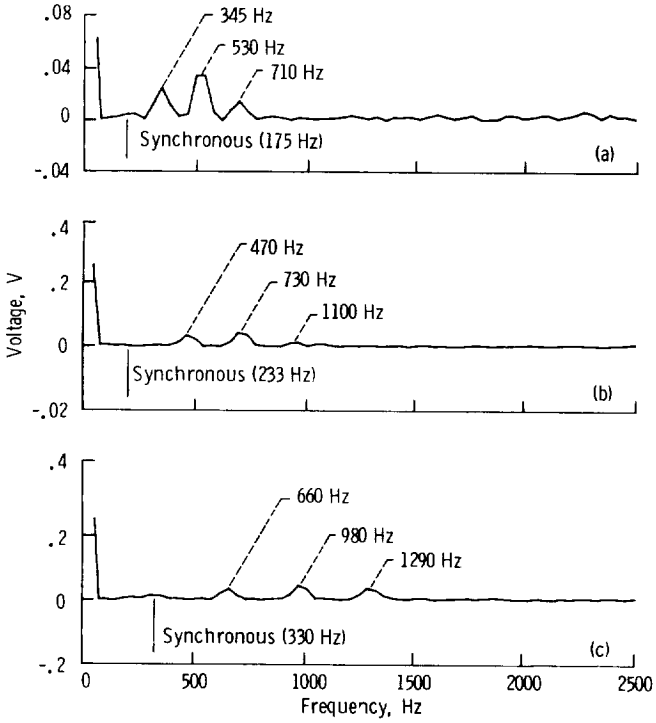

(a) Shaft speed, 10 500 rpm.
(b) Shaft speed, 14 000 rpm.
(c) Shaft speed, 19 800 rpm.

Figure 28.—Fast Fourier transform of film thickness (probe 1) for outward-pumping spiral-groove seal, segmented secondary seal, steady seal seat mode, and true seal seat.

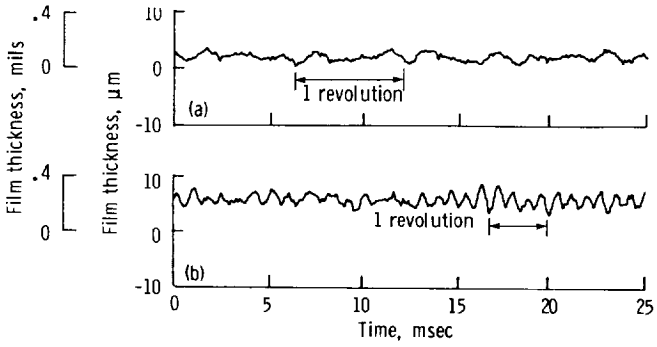

(a) Shaft speed, 10 500 rpm.
(b) Shaft speed, 19 800 rpm.

Figure 29.—Film thickness as function of time (probe 1) for outward-pumping spiral-groove seal, segmented secondary seal, sinusoidal seal seat mode (50-μm (2-mil) amplitude at 100 Hz), and true seal seat.

was stable and was 3.1 N-cm (0.28 in.-lb) for 10 500 rpm and 3.4 N-cm (0.30 in.-lb) for 19 800 rpm, with no indication of seal face rubs.

The film thickness responses for the steady mode were compared for the true and skewed seal seats at 19 800 rpm (fig. 30). The film thickness amplitude was 7 μm (0.3 mil) for the skewed seal seat and 2.5 μm (0.1 mil) for the true seal seat. Thus the primary ring did not track the swashing motion

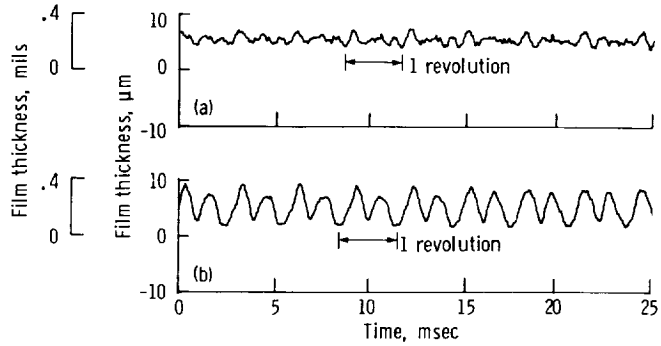

(a) True seal seat.
(b) Skewed seal seat.

Figure 30.—Film thickness as function of time (probe 1) for outward-pumping spiral-groove seal, segmented secondary seal, steady seal seat mode, and 19 800-rpm shaft speed.

of the skewed seat. As mentioned previously, perfect tracking would be indicated by a straight line in these traces. The film thickness frequency was two times synchronous.

The primary ring tilt angle (fig. 18) was plotted as a function of time for the steady mode with true seal seat at 19 800 rpm (fig. 31). As previously mentioned, the tilt angle is an indication of the rocking motion of the primary ring with respect to the seal seat. These angles were calculated as described for the inward-pumping seals. The tilt angles plotted about two mutually perpendicular axes x and y, respectively (figs. 31(a) and (b)), showed a complex waveform approximately two times synchronous. The resultant tilt angle (fig. 31(c)) indicated a variation of approximately 0.003° peak to peak at four times synchronous.

The tilt angles for the steady mode with skewed seal seat at 19 800 rpm (fig. 32) were similar to those in the previous case (fig. 31). However, the resultant amplitudes were 0.006° peak to peak for the skewed seal seat (fig. 32(c)) versus 0.003° for the true seal seat (fig. 31(c)). Thus the skewed seal seat caused the primary ring tilt angle to go through greater excursions. The seal seat motion for this mode (fig. 33, probes 5, 8, and 11) indicated the axial motion of the seal seat. Because they are out of phase, the traces suggest a swashing motion of the seal seat. (As mentioned previously, in-phase traces would indicate pure axial translation.) The amplitude was 50 μm (2 mils) at synchronous frequency. The seal frictional torque was 3.4 N-cm (0.30 in.-lb) for both the true and skewed seal seats. The torque was stable with no evidence of rubbing during these tests.

The film thickness response to the true and skewed seal seats was determined for the sinusoidal seal seat mode at 19 800 rpm (fig. 34). These traces are similar to the response for the steady mode (fig. 30), indicating no difference in tracking ability between the steady and sinusoidal seal seat modes. The seal seat axial motion for the sinusoidal mode with true seal seat (fig. 35) was not a perfect sinusoid because of servovalve limitations. This is the seal seat motion associated with figure 34(a). The seal seat axial motion for the sinusoidal seal seat

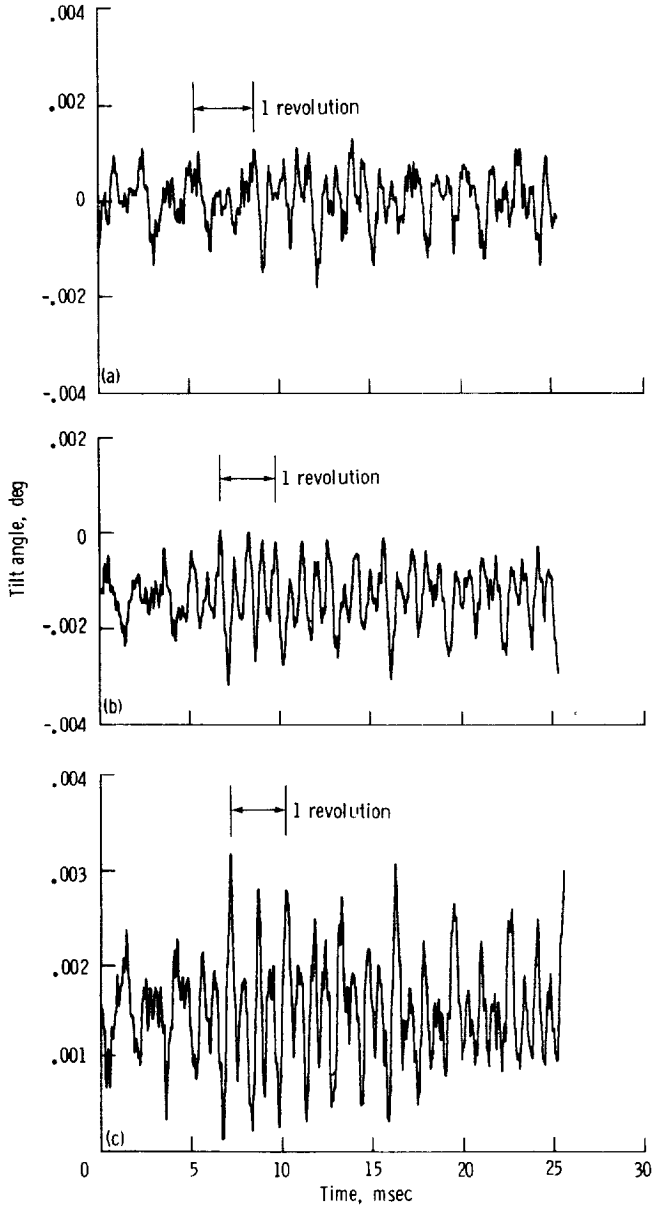

(a) Tilt angle about x axis (β_x).
(b) Tilt angle about y axis (β_y).
(c) Resultant tilt angle.

Figure 31.—Tilt angle as function of time for outward-pumping spiral-groove seal, segmented secondary seal, steady seal seat mode, true seal seat, and 19 800-rpm shaft speed.

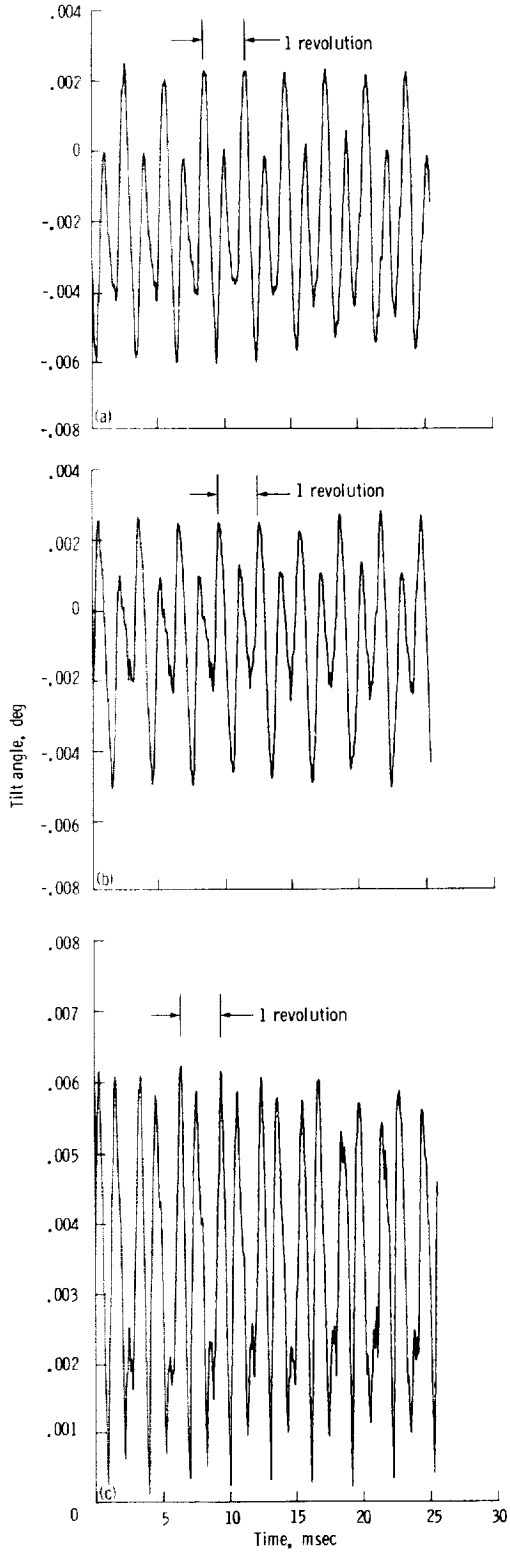

(a) Tilt angle about x axis (β_x).
(b) Tilt angle about y axis (β_y).
(c) Resultant tilt angle.

Figure 32.—Tilt angle as function of time for outward-pumping spiral-groove seal, segmented secondary seal, steady seal seat mode, skewed seal seat (0.028° skew), and 19 800-rpm shaft speed.

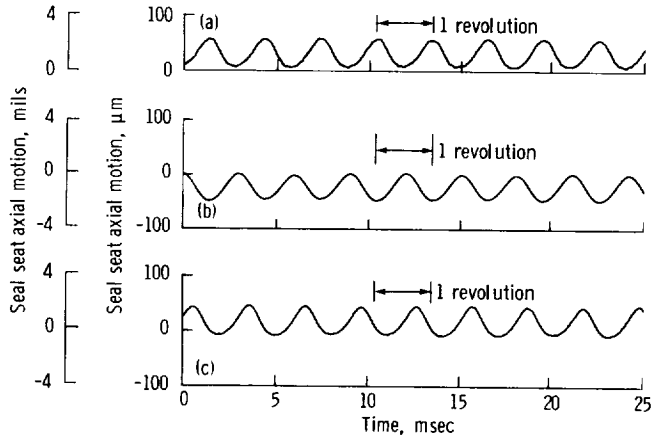

(a) Probe 5.
(b) Probe 8.
(c) Probe 11.

Figure 33.—Seal seat axial motion for skewed seal seat mode (0.028° skew angle), steady seal seat mode, and 19 400-rpm shaft speed.

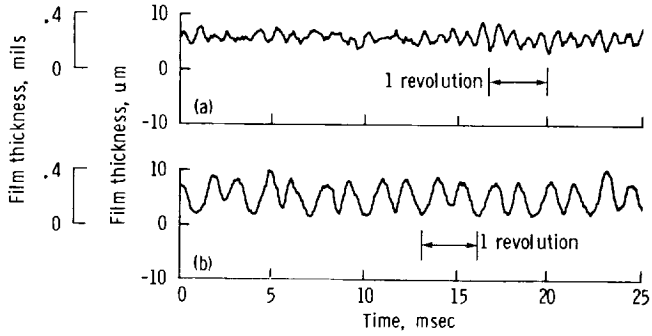

(a) True seal seat.
(b) Skewed seal seat (0.028° skew angle).

Figure 34.—Film thickness as function of time (probe 1) for outward-pumping spiral-groove seal, segmented secondary seal, sinusoidal seal seat mode (50-µm (2-mil) amplitude at 100 Hz), and 19 800-rpm shaft speed.

mode with skewed seal seat (fig. 36) had a complex waveform composed of the swashing motion caused by the skewed seat superimposed on the sinusoidal axial motion of the seal seat. This is the seal seat motion associated with figure 34(b). The seal frictional torque for these cases was 3.4 N-cm (0.30 in.-lb) and was stable with no evidence of seal face rubs during these runs.

During the tests of the outward-pumping spiral-groove seal for the steady seal seat mode with the skewed seal seat, the film thickness was unstable at 14 000 rpm when the axial load was set at approximately 68.9 N (15.5 lb). At these conditions very severe rubbing took place, and the seal frictional torque spiked erratically, accompanied by large fluctuations in shaft speed. The speed was then increased to 19 500 rpm, and an axial load of 84.5 N (19 lb) was achieved before the seal encountered similar instability. With the true seal seat this seal supported these axial loads with no signs of seal face rubbing.

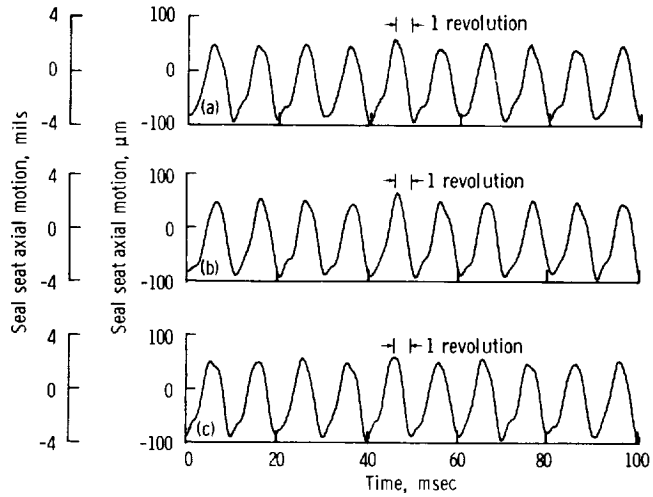

(a) Probe 5.
(b) Probe 8.
(c) Probe 11.

Figure 35.—Seal seat axial motion for sinusoidal seal seat mode (50-µm (2-mil) amplitude at 100 Hz), true seal seat, and 19 800-rpm shaft speed.

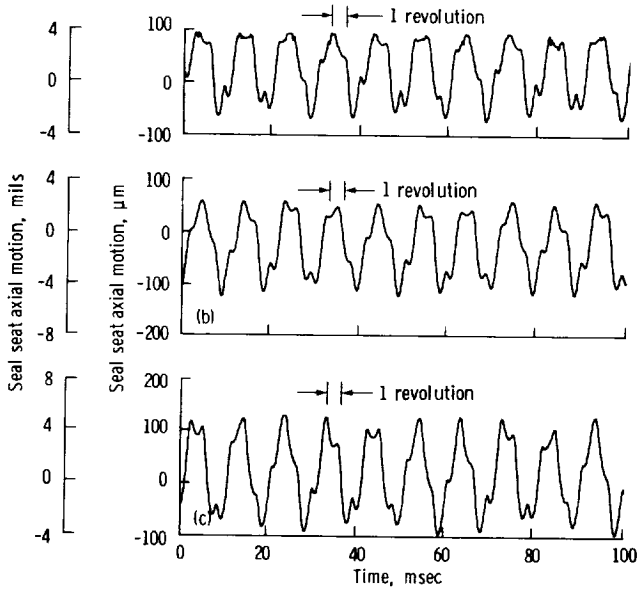

(a) Probe 5.
(b) Probe 8.
(c) Probe 11.

Figure 36.—Seal seat axial motion for combined skewed seal seat and sinusoidal seal seat modes. Skewed seal seat (0.028° skew angle), sinusoidal seal seat mode (50-µm (2-mil) amplitude at 100 Hz), and 19 400-rpm shaft speed.

The inward-pumping spiral-groove seal (with true seal seat) also supported these loads with no signs of rubbing or instability. It appeared that skewed seal seats seriously affected the load-carrying capacity and stability of self-acting seals. On the other hand, the self-acting seals had excellent ability to track pure axial translations of the seal seat if the seal seat

was not skewed. This was due to the strong squeeze-film action for the true seal seat case.

Comparison of Experimental and Analytical Data

Attempts at comparing measured film vibrations with analytical values were unsuccessful; therefore no comparisons are shown in this report. For instance, the analytical film thickness response to the sinusoidal seal seat axial motion mode showed no rocking motion of the seal seat, which is true since there is no force or moment that would cause this motion for this mode. The experimental data on the other hand showed significant rocking motion for the sinusoidal seal seat mode because of unavoidable misalignment and imperfection in manufacturing the parts (real-world effects).

For the skewed seal seat mode numerical instabilities in the computer program precluded obtaining results for seal seat skew angles above approximately 0.0035°. This represents a skew of approximately 5 μm (0.2 mil) across the seal diameter. The experimental data, however, showed that the seal performed without rubbing (at reduced axial load) even at a skew angle of 0.03° (50 μm (2 mils) across the seal diameter). Comparison of analytical values with experimental data for skew angles of the order of 0.0035° (the range where analytical values were obtainable) was not possible because random motions and misalignment of experimental hardware were of this order. This precluded a direct comparison of experiment and analysis. One way around this problem would be to use the seal seat motions defined in this report as a forcing function input to an analytical model and compare the analytical and experimental results. This was not done, but it would be a means of developing an analytical model that would reliably predict the dynamic performance of self-acting seals.

Summary of Results

Experimental tests were performed on an inward- and an outward-pumping spiral-groove face seal to gain insight into the dynamic characteristics of the film thickness. Film thickness response for four seal seat vibratory modes was recorded as a function of time. These modes were (1) steady seal seat mode with true seal seat (baseline), (2) sinusoidal seal seat mode with true seal seat, (3) steady seal seat mode with skewed seal seat, and (4) sinusoidal seal seat mode with skewed seal seat. The amplitude and frequency of the sinusoidal motion were 50 μm (2 mils) and 100 Hz for the sinusoidal seal seat mode cases.

The effect of secondary seal friction on film thickness dynamics was also evaluated for three secondary seal configurations: (1) a segmented secondary seal, (2) a variable-friction secondary seal, and (3) no secondary seal.

The tilt angle (angle between the seal seat and the primary ring faces) was calculated for various cases from the measured film thickness data and plotted as a function of time. The tilt angle gave a graphic indication of the primary ring motion.

The significant findings from the tests were as follows:

1. The primary ring followed the pure axial sinusoidal oscillations of the seal seat very well with no evidence of face contact for both the inward- and outward-pumping seals. This conclusion was reached because the film thickness response was the same for both large sinusoidal axial translations of the seal seat and for no translation of the seal seat.
2. For the outward-pumping seal the primary ring did not follow the swashing motion of the seal seat when the seal seat was skewed with respect to the shaft axis of rotation. This was concluded because the film thickness as a function of time had significantly higher amplitudes than it did for the true seal seat. Note that the inward-pumping seal was not tested with a skewed seal seat; however, the same results are anticipated for the inward-pumping seal.
3. Seal seats that were skewed with respect to the shaft axis of rotation seriously degraded the load-carrying capacity of the spiral-groove seal (i.e., face contact occurred at lower film axial loads).
4. For the inward-pumping seal operating at a film axial load of 73 N (16.4 lb) with no secondary seal, the film vibration amplitude was less than for the segmented secondary seal. However, for higher film axial load (89 N; 20 lb) and speed (20 000 rpm) the seal became unstable when running with no secondary seal but was stable at this load when running with the segmented secondary seal. This indicated that higher levels of secondary seal friction are necessary at higher film loads and speeds.
5. For the inward-pumping seal the onset of instability (seriously deteriorated performance) for the steady mode occurred when the secondary seal static friction was 27 to 40 N (6 to 9 lb). Below this range the seal was relatively insensitive to friction.
6. Varying secondary seal friction had the effect of changing the axial load on the film; higher friction caused higher film loads.
7. For the inward-pumping seal operating in the sinusoidal seal seat mode, film thickness dynamic response was insensitive to the amplitude and frequency of the seal seat oscillation over the test range (for amplitudes to 50 μm (2 mils) and frequencies to 100 Hz). Film thickness dynamic response was also insensitive to film axial load for the test range 73 to 96 N (16.4 to 21.5 lb).

Further work should be done to evaluate the effect of a skewed seal seat on self-acting seal dynamics. This work should include the development of mathematical models in parallel with experimental models with which to validate the

mathematical models. Experimental validation of mathematical models requires that the rig and seal hardware be nearly perfect since manufacturing imperfections of the order of the film thickness (5 μm, 0.2 mil) adversely affect film thickness response. Also, the effect of secondary seal friction must be evaluated to establish stability boundaries for various film loadings.

Lewis Research Center
National Aeronautics and Space Administration
Cleveland, Ohio, September 3, 1985

References

1. DiRusso, E.: Film Thickness Measurement for Spiral Groove and Rayleigh Step Lift Pad Self-Acting Face Seals. NASA TP-2058, 1982.
2. DiRusso, E.: Dynamic Behavior of Spiral-Groove and Rayleigh-Step Self-Acting Face Seals. NASA TP-2266, 1984.
3. Etsion, I.: Dynamic Analysis of Noncontacting Face Seals. J. Lubr. Technol., vol. 104, no. 4, Oct. 1982, pp. 460–468.
4. Etsion, I: Squeeze Film Effects in Radial Face Seals. NASA CR-135415, 1978.
5. Ludwig, L.P.: Self-Acting Shaft Seals. NASA TM-73856, 1978.
6. Ludwig, L.P.; and Greiner, H.F.: Design Considerations in Mechanical Face Seals for Improved Performance, 1—Basic Configurations. Mech. Eng., vol. 100, no. 11, Nov. 1978, pp. 38–46.
7. Ludwig, L.P.; and Greiner, H.F.: Design Consideration in Mechanical Face Seals for Improved Performance, 2—Lubrication. Mech. Eng., vol. 100, no. 11, Dec. 1978, pp. 18–23.
8. DiRusso, E.: Design Analysis of a Self-Acting Spiral Groove Ring Seal for Counter-Rotating Shafts. AIAA Paper 83-1134, June 1983.
9. DiRusso, E.: Feasibility Analysis of a Spiral Groove Ring Seal for Counter-Rotating Shafts. J. Aircr., vol. 21, no. 8, Aug. 1984, pp. 618–622.
10. DiRusso, E.: Variable Friction Secondary Seal for Face Seals. NASA-CASE-LEW-14170-1, Nov. 16, 1984. (U.S. Patent Application SN-672224.)

1. Report No.	2. Government Accession No.	3. Recipient's Catalog No.
NASA TP-2544		

4. Title and Subtitle	5. Report Date
Dynamic Response of Film Thickness in Spiral-Groove Face Seals	December 1985
	6. Performing Organization Code 505-33-7B
7. Author(s) Eliseo DiRusso	8. Performing Organization Report No. E-2683
	10. Work Unit No.
9. Performing Organization Name and Address National Aeronautics and Space Administration Lewis Research Center Cleveland, Ohio 44135	11. Contract or Grant No.
	13. Type of Report and Period Covered Technical Paper
12. Sponsoring Agency Name and Address National Aeronautics and Space Administration Washington, D.C. 20546	14. Sponsoring Agency Code

15. Supplementary Notes

16. Abstract

Tests were performed on an inward- and an outward-pumping spiral-groove face seal to experimentally determine the film thickness response to seal seat motions and to gain insight into the effect of secondary seal friction on film thickness behavior. Film thickness, seal seat axial motion, seal frictional torque, and film axial load were recorded as functions of time. The experiments revealed that for sinusoidal axial oscillations of the seal seat, the primary ring followed the seal seat motion very well. For a skewed seal seat, however, the primary ring did not follow the seal seat motion, and load-carrying capacity was degraded. Secondary seal friction was varied over a wide range to determine its effect on film thickness dynamics. The seals were tested with ambient air at room temperature and atmospheric pressure as the fluid medium. The test speed ranged from 7000 to 20 000 rpm. Seal tangential velocity ranged from 34 to 98 m/sec (113 to 323 ft/sec).

17. Key Words (Suggested by Author(s))	18. Distribution Statement
Face seals Self-acting seals Gas bearings Gas film thickness Spiral-groove seal	Unclassified - unlimited STAR Category 07

19. Security Classif. (of this report)	20. Security Classif. (of this page)	21. No. of pages	22. Price
Unclassified	Unclassified	21	A02

For sale by the National Technical Information Service, Springfield, Virginia 22161

NASA-Langley, 1985